Journal of Alloys and Compounds 722 (2017) 953–961

Contents lists available at ScienceDirect

Journal of Alloys and Compounds

journal homepage: http://www.elsevier.com/locate/jalcom

Pressure-induced structural changes in Methylamine borane and dimethylamine borane

Petra Á. Szilágyi [a, *], Steven Hunter [b, c], Carole A. Morrison [b], Chiu C. Tang [d], Colin R. Pulham [b, c]

[a] University of Greenwich, Medway Campus, Chatham, ME4 4TB, UK
[b] School of Chemistry and EaStCHEM Research School, University of Edinburgh, The King's Buildings, West Mains Road, Edinburgh, EH9 3JJ, UK
[c] Centre for Science at Extreme Conditions, The University of Edinburgh, Mayfield Road, Edinburgh, EH9 3JZ, UK
[d] Diamond Light Source Ltd, Harwell Science and Innovation Campus, Didcot, Oxfordshire, OX11 0DE, UK

ARTICLE INFO

Article history:
Received 26 April 2017
Received in revised form
14 June 2017
Accepted 15 June 2017
Available online 17 June 2017

The paper has been presented in Symposium O: Functional metal hydrides, at the E-MRS Fall Meeting and Exhibit, Warsaw, September, 2016.

Keywords:
Hydrogen storage
Phase transition
High pressure
Synchrotron X-ray powder diffraction

ABSTRACT

Methylamine borane and dimethylamine borane have been studied under compression to 3 GPa using Raman spectroscopy and synchrotron powder X-ray diffraction. Both undergo reversible pressure-induced structural changes in this pressure range. The structural changes in the case of methylamine borane may be indicative of a second-order phase transition, taking place between *ca.* 0.8–1.2 GPa, which does not result in a change of space-group symmetry. In the case of dimethylamine borane, however, a reversible, reconstructive phase transition (monoclinic → orthorhombic) occurs below 0.7 GPa. This new high-pressure phase was successfully indexed, with a possible space group assignment of *Pccn* or *Pbcn*.

1. Introduction

With increasing demands on fossil fuels, many industrialised nations are turning towards alternative sources of energy. The "hydrogen economy", in which hydrogen is used as a "green" feedstock in fuel cells to power motor vehicles, homes, *etc.* has been highlighted as a potential solution to the energy problem. Challenges to be faced before this becomes a reality include the development of sustainable methods of hydrogen production that do not involve fossil fuels, and the safe and reversible storage of hydrogen [1–4]. Several promising areas have been identified, especially in the use of solid hydrogen-containing materials. Although these materials contain substantial amounts of hydrogen by weight percent, release of hydrogen gas is often difficult to achieve on account of the high stability of these materials with respect to decomposition. Experimental efforts are therefore focussed on catalytic or chemical-doping methods to destabilise these hydrides using a range of empirical approaches [5–7]. An important step in developing an understanding of the chemical properties of such materials is the study of structure, with a particular focus on the structural response as a function of both temperature and pressure. In addition to developing an understanding of the relationship between structure and the potential for hydrogen-storage, variable temperature and pressure studies may also result in the formation of new phases with enhanced properties that may be recovered in bulk quantities at ambient conditions [8,9].

Experimental mapping of polymorphism for light hydrides using X-rays is not a trivial task due to the presence of weakly scattering hydrogen atoms. Furthermore, many of these materials are polycrystalline and highly hygroscopic, which makes obtaining good quality powder diffraction data challenging. Using powder X-ray diffraction to identify and solve polymorphism of light hydrides under pressure is further complicated by the possibility of multiple

* Corresponding author.
E-mail address: P.A.Szilagyi@greenwich.ac.uk (P.Á. Szilágyi).

http://dx.doi.org/10.1016/j.jallcom.2017.06.174
0925-8388/

fits to the resulting pattern, which makes the use of complementary techniques indispensable. Neutron powder diffraction studies are also hindered by strong absorption from the 20% abundance of ^{10}B nuclei and incoherent scattering from ^{1}H, thereby requiring the synthesis of both ^{11}B and ^{2}H isotope-enriched samples [10]. This can be both time-consuming and expensive. On the other hand, Raman spectroscopy can help reveal crucial structural information at the molecular level [11]. Theoretical modelling also yields structural information, but it may also prove to be rather challenging as seen from the apparent disagreement between the observed and theoretically predicted structures for $LiBH_4$ [12–14] and $Mg(BH_4)_2$ [15–18].

In this work, we present a study combining intense synchrotron powder diffraction and Raman spectroscopy, aimed at exploring the structural properties of methylamine borane and dimethylamine borane. First-principles simulations were performed to aid the assignment of the Raman spectra. Ammonia borane has been highlighted as a promising material for chemical hydrogen-storage applications [19–23]. Containing three protic N–H and three hydridic B–H bonds and having a low molecular weight, it has the potential to meet the rigorous gravimetric and volumetric hydrogen-storage capacity requirements for mobile applications. It has therefore been extensively studied. It is known that thermal decomposition results in the release of hydrogen in several steps between 100 and 500 °C [24]. Infusion of NH_3BH_3 in mesoporous silica, carbon cryogel, and metal-organic frameworks was found to increase the dehydrogenation kinetics and also to suppress borazine formation (a toxic by-product) [25–29]. Dissociation of NH_3BH_3 is also reported to be activated by the addition of cation exchange resins, zeolites and ionic liquids [30–32].

Because of the presence of B–H···H–N bonds in solid-state ammonia borane, its behaviour under pressure has also been investigated with a variety of methods, such as Raman spectroscopy [33–36], X-ray [37–39] and neutron diffraction [39–41], and computational methods [42–46]. It should be noted that owing to the intrinsic softness of ammonia borane most studies did not use any pressure-transmitting medium except for that by Custalcean et al. [47], in which hydrostatic conditions were thus ensured. Raman studies have suggested phase transitions at 2.0, 5.0 and 12.0 GPa, and combined data from neutron and X-ray diffraction have found a body-centred tetragonal *I*4*mm* ambient phase that undergoes a transition into a *Cmc*2$_1$ orthorhombic phase at *ca.* 1.2 GPa, which subsequently transforms into a *P*1 triclinic phase at approximately 8.2 GPa [37,40,48–50].

N-substituted ammonia borane derivatives, such as methylamine borane and dimethylamine borane [$CH_3NH_2BH_3$ and $(CH_3)_2NHBH_3$] have theoretical hydrogen capacities of 17.9 and 17.0 wt%, respectively, of which 9.0 and 6.8 wt% hydrogen is experimentally available [51–53]. Furthermore, Sun and co-workers have pointed out that *N*-methyl substitution of ammonia borane enhances the reversibility of the system and prevents the formation of diborane and ammonia – two major contaminants in the case of ammonia borane [54]. Dimethylamine borane is also of great interest as it is known to undergo dehydrogenation in the presence of transition-metal catalysts to give hydrogen gas and the cyclic (dimethylamino)borane dimer, $(Me_2NBH_2)_2$, as final products [55–67].

Despite the high hydrogen content, the presence of non-classical B–H···H–N bonds in solid methylamine and dimethylamine borane [68], and the effort invested in the study of ammonia borane, there has been only one Raman-spectroscopy study published on the behaviour of dimethylamine borane under pressure using [69]. In this paper, we report the structural changes occurring in the methylamine borane and *N*,*N*-dimethylamine borane systems under quasi-hydrostatic pressure up to 3 GPa.

2. Experimental

All chemicals were purchased from Sigma Aldrich and were used without further purification before syntheses.

2.1. Synthesis of methylamine borane

0.4266 g (11 mmol) sodium tetrahydridoborate was mixed with 0.8381 g (12 mmol) methylammonium hydrochloride in 20 cm^3 anhydrous THF under N_2 atmosphere in a reaction vessel equipped with a gas bubbler, similar to the procedure explained by Bowden et al. [51]. Formation of H_2 gas was observed immediately after the addition of the reactants into the vessel. The reaction mixture was stirred under constant N_2-flow at 45 °C for 2 h, the heating and gas-flow were then stopped and the mixture was left stirring overnight at ambient temperature. The resultant slurry was then filtered off and washed with 3 cm^3 anhydrous THF under N_2-atmosphere. The filtered solution was then evaporated under vacuum and white, polycrystalline methylamine borane was obtained, which was characterised by Raman spectroscopy.

2.2. Synthesis of dimethylamine borane

Dimethylamine borane was prepared using the same protocol as for the methylamine borane by the use of 0.4744 g (12 mmol) sodium tetrahydridoborate and 1.0093 g (12 mmol) dimethylammonium hydrochloride. The resulting white polycrystalline material was also characterised by Raman spectroscopy.

2.3. High-pressure measurements: general procedures

High-pressure Raman spectroscopy and X-ray diffraction experiments were performed using a Merrill-Bassett diamond-anvil cell (40° half-opening angle), equipped with 600 μm culets and a tungsten gasket with a 300 μm hole [70]. The sample and a chip of ruby (as a pressure calibrant) were loaded into the diamond-anvil cell with Fluorinert (FC-77) as a pressure-transmitting medium. This was chosen as the samples were found to be soluble in other media such as mixed pentanes, glycerin and methanol-ethanol mixtures. Furthermore, they decompose in methanolic solutions. The induced pressure was determined by monitoring the ruby crystal R_1 fluorescence wavelength by fitting Lorentzian lineshapes to the R_1 line: the resulting uncertainty is ±0.04 GPa [71].

2.4. Raman Spectroscopy

Raman measurements were conducted at ambient temperature on the powdered samples. Spectra were recorded on a LabRam instrument equipped with a 50 mW He-Ne laser of wavelength 632.8 nm.

2.5. Synchrotron X-ray powder diffraction (SXPD) data collection

Diffraction data was collected on beamline I11 at the Diamond Light Source [72] using a monochromatic X-ray beam of $\lambda = 0.48512$ Å. A mar345 image plate was used to collect angle-dispersive diffraction patterns. The sample-to-detector distance and the wavelength were calibrated using a CeO_2 powder standard. The pressure was measured ex-situ using ruby fluorescence lines from small embedded crystals in the sample before collecting each diffraction pattern. The data was integrated using the program Fit2D [73] with masks to avoid integration of regions of the detector shaded by the body of the pressure cell.

2.6. Structure analysis, reduction and refinement

Space groups and unit cells of the materials under study were determined from the powder patterns by indexing software Crysfire [74], verified by LeBail refinement in GSAS [75] analytical software. Single-crystal structures as determined by Bowden and co-workers [51] for the methylamine borane and by Aldridge et al. [68] for the dimethylamine borane were used as models in FOX 1.7.7.7-R1013 [76]. This data was then re-loaded into GSAS and Rietveld refinements were carried out on the heavy atoms, first with constraints applied on the bond lengths and angles which were gradually lifted. Hydrogen atoms were then added in the structure, in accordance with the molecular geometry calculation in WinCrystals 2000 [77]. The resulting crystallography information file was re-loaded into GSAS and the final Rietveld refinement carried out by first handling the molecular structure as a rigid body (in effect fixing the hydrogen atom positions). All constraints were then gradually released as the least-squares fitting procedure converged on a minimum structure.

2.7. Computational methods

Structure optimisations were performed using density functional theory (DFT) and the plane-wave pseudopotential method as implemented in CASTEP version 5.5 [78]. Following geometry optimisation, phonon frequencies were calculated using the finite displacement method, as executed within the CASTEP code. Visualisation of individual wave-vectors, which allowed mode assignment, were performed using the Jmol software package [79].

3. Results and discussion

3.1. Methylamine borane

Raman Spectroscopy. The Raman spectrum of methylamine borane at ambient pressure (Fig. 1) shares many features with that of solid ammonia borane [80]. To aid interpretation, the spectrum was compared with the computationally calculated eigenvalues, where agreement was observed for all modes to within 4%. The major difference between the spectrum of methylamine borane and that of ammonia borane arises from the presence of the methyl group in the former. In addition, the characteristic bands for the B–N-stretching mode with isotope splitting are at somewhat lower wavenumbers in the case of methylamine borane (738 and 753 cm^{-1}) than for ammonia borane [80] (784 and 800 cm^{-1}). A full listing of assigned vibrational modes is available in Table A1 of the Supplementary Information.

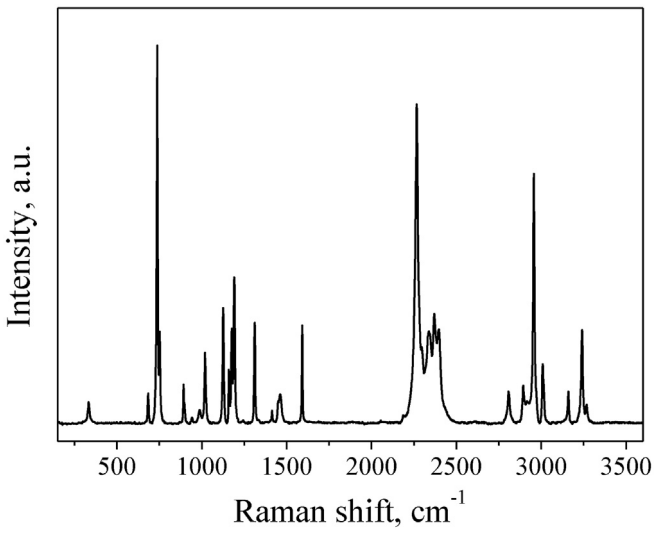

Fig. 1. Ambient-temperature Raman spectrum of $CH_3NH_2BH_3$.

On increasing the pressure, spectral changes, indicative of structural variation in the condensed phase of methylamine borane were observed (see Fig. 2a and c). In general, all modes blue-shifted (hardened) with respect to external pressure, but those involved with the intermolecular dihydrogen bonds (the N–H stretching and deformation modes) red-shifted (softened). The same pressure-induced phenomenon of mode softening was observed for ammonia borane and it was interpreted as being indicative of the strengthening of the dihydrogen bonds in the solid state, which consequently results in the weakening of the N–H bonds [34,47]. In addition, for the N–H scissoring mode we note that the corresponding band does not split into two at higher pressures, as observed for ammonia borane.

The evolution of Raman modes as a function of applied pressure shows some changes taking place in the 1–1.5 GPa region. Close to linear plots were obtained for $\partial\overline{\nu}/\partial p$ with slight divergence at pressures above 1.5 GPa for modes in the region of 3130–3350 cm^{-1} and 1430-1620 cm^{-1} (see Fig. 2b and d). This discrepancy between the Raman peak maxima at the low- and high-pressure regions may be indicative of pressure-induced structural changes.

Structural Characterisation: Synchrotron X-ray Diffraction. The structure of methylamine borane was first determined by M. E. Bowden and co-workers at 113 K using single-crystal diffraction [78]. The authors found that the compound crystallises in the orthorhombic *Pnma* space group and also identified the presence of intermolecular B–H···H–N dihydrogen bonds (2.218 Å). Visualisation of the molecular packing in Mercury [81] reveals interchain B–H···H–C interactions of 2.764 Å and C–H···H–C interactions of 2.800 Å [51]. Single-crystal data (150 K) were collected on the compound by S. Aldridge et al. (Fig. 3). They found that molecules of the methylamine borane adduct are linked in ribbons running along the *b*-axis and within these ribbons pairs of molecules are aligned in an antiparallel fashion, with the B–N bonds along the *c*-axis. Visualisation of their single-crystal data shows that each pair of molecules is linked by two B–H···H–N dihydrogen bonds of 2.130 Å and that the ribbons are linked in a layer through B–H···H–N contacts of 2.504 Å, and B–H···H–C interactions of 2.763 and 2.979 Å which hold the layers together [68].

SXPD data were collected on polycrystalline methylamine borane at ambient temperature, as a function of pressure up to 3.0 GPa. The resulting patterns (Fig. 4) indicate that peaks shift to higher 2θ values with increasing pressures, as expected. As no peaks appear or disappear upon changing pressure, we can safely conclude that there is no pressure-induced first-order phase transition taking place in the condensed phase of methylamine borane at ambient temperature conditions, up to 3.0 GPa.

In order to verify whether second-order phase transitions have taken place in methylamine borane system each of the diffractions patterns was fitted to model structures. Lattice parameters for all the patterns have been successfully refined using the orthorhombic (*Pnma*) structure of the ambient-pressure form as the starting structural model (see Table 1).

Compression plots of the lattice parameters and the cell volume (Fig. 5) show some changes in their gradients between *ca.* 0.8 and 1.5 GPa. This suggests that, while there is no reconstructive first-order phase transition occurring in the system up to 3 GPa, pressure-induced structural changes or even a second-order phase transition may have occurred over this pressure range.

Taking a closer look at the compression plots of the lattice

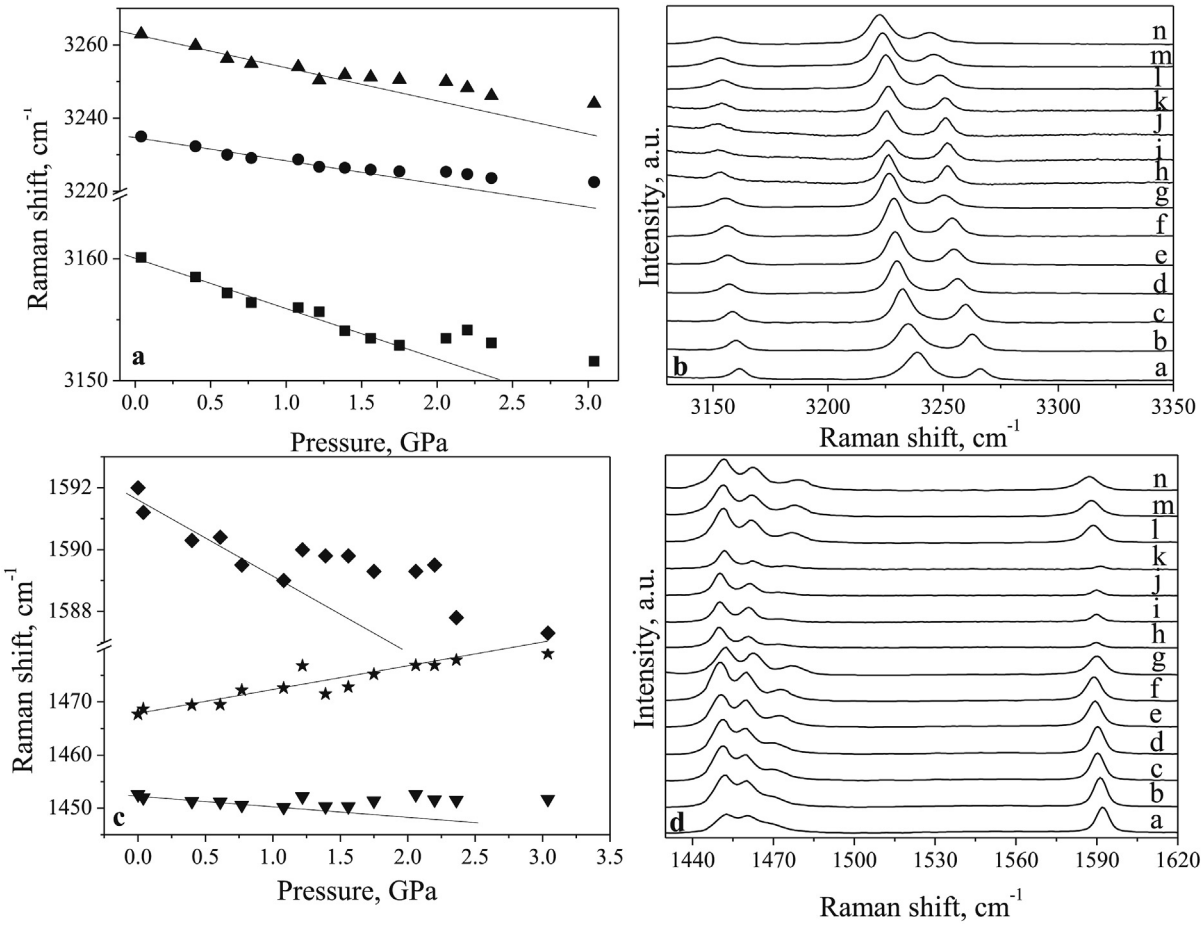

Fig. 2. Changes in the Raman spectra for methylamine borane with respect to pressure **(a)** 3130-3350 cm^{-1} region ▲ NH_2 asymmetric stretch, • NH_2 symmetric stretch, and ■ BH_3 symmetric stretch + NH_2–BH_3–CH_3 wag, **(c)** 1430-1620 cm^{-1} region ◆ NH_2 scissor, ★CH_3 scissoring, and ▼ CH_3 twist, **(b)** and **(d)** pressure range (in GPa): a:0; b:0.04; c:0.4; d:0.6, e:0.8, f:1.1, g:1.2; h:1.4; i:1.6; j:1.8; k:2.1; l:2.2; m:2.4; n:3.0.

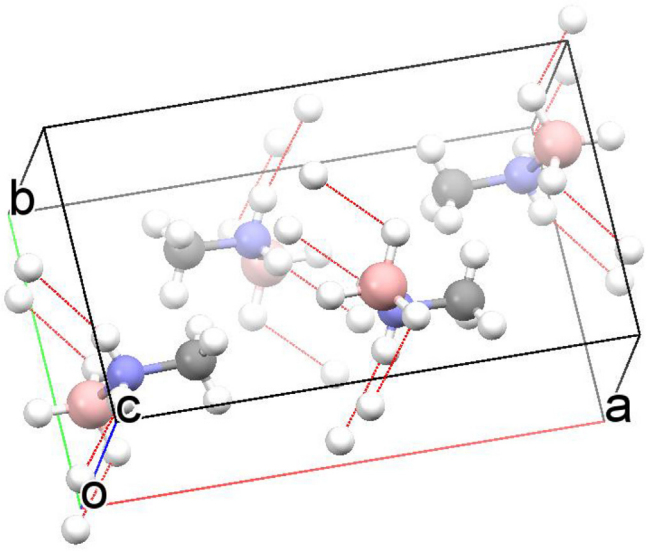

Fig. 3. Crystal packing of $CH_3NH_2BH_3$ at ambient pressure highlighting the B–H···H–N contacts.

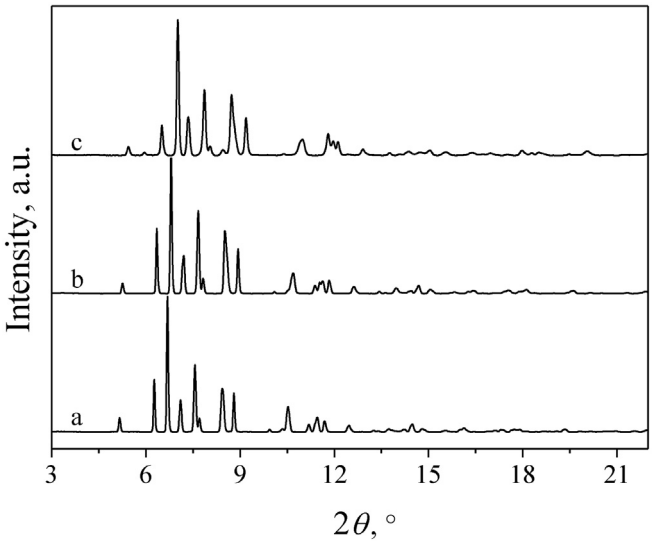

Fig. 4. Powder X-ray patterns of $CH_3NH_2BH_3$ at pressures of (a) 0.7 GPa, (b) 1.5 GPa and (c) 3.0 GPa.

parameters (Fig. 5a), we observe that the low and high-pressure trends differ the most along the *b*-axis. This coincides with the direction of the N–H···H–B dihydrogen bonds, as determined by Aldridge and co-workers [68]. It is also worth noting that the N–H

Table 1
Refined structural parameters for the CH_3NHBH_3 as a function of pressure.

Pressure, GPa	a, Å	b, Å	c, Å	V_{cell}, Å^3
0 [51]	11.099	6.584	4.919	359.460
0 [68]	11.135	6.558	4.919	359.204
0	11.164 (2)	6.7384 (7)	4.9708 (7)	373.927 (2)
0.4	10.972 (1)	6.6681 (2)	4.9247 (4)	360.317 (1)
0.7	10.718 (3)	6.584 (2)	4.871 (1)	343.743 (3)
0.8	10.664 (3)	6.558 (1)	4.854 (1)	339.467 (3)
1.2	10.516 (7)	6.555 (3)	4.817 (2)	332.035 (7)
1.5	10.489 (2)	6.4963 (9)	4.8036 (6)	327.319 (2)
1.8	10.361 (4)	6.439 (2)	4.771 (1)	318.302 (4)
2.3	10.285 (9)	6.390 (4)	4.743 (4)	311.715 (9)
3	10.128 (9)	6.343 (4)	4.698 (3)	301.783 (9)

and B—H stretching and deformation modes were found to undergo the most significant changes in the Raman spectra above 1 GPa. In addition, up to 3.0 GPa, the *a*-axis was found to be around 1.65 times more compressible than both the *b* and *c* axes. The difference in compressibility along the *a*-axis can be explained by close inspection of the crystal packing of methylamine borane (Fig. 3) [68]. The nearest intermolecular heavy-atom distance occurring along the direction of the *a*-axis in the ambient pressure structure is $d_{C\ldots N}$ = 4.239 Å, while for the *b*- and *c*-axes they are substantially shorter: $d_{B\ldots N}$ = 3.509 Å and $d_{B\ldots N}$ = 3.448 Å, respectively [68].

Compression plots of the cell parameters thus suggest that there may be pressure-induced structural changes in the 0.8–1.2 GPa range. The compression plot of the cell volume (Fig. 5b) also suggests that the compressibility of the unit cell differs in the low-pressure and high-pressure regions.

It should be noted that at these pressures the pressure-transmitting medium used should no longer be hydrostatic (Fluorinert FC77 is hydrostatic up to only 1.0 GPa) [82], which implies that its use may have introduced pressure-related stress gradients within the diamond-anvil cell. However, no signs of broadening of the diffraction peaks or broadening of the ruby fluorescence line were observed, suggesting that, at least for these low pressures, the intrinsic softness of the sample retains hydrostatic conditions.

The Raman spectroscopic and SXPD data all suggest the existence of pressure-induced structural changes in the methylamine borane system at ambient temperature around 1.2 GPa. These changes may also be indicative of a second-order phase transition.

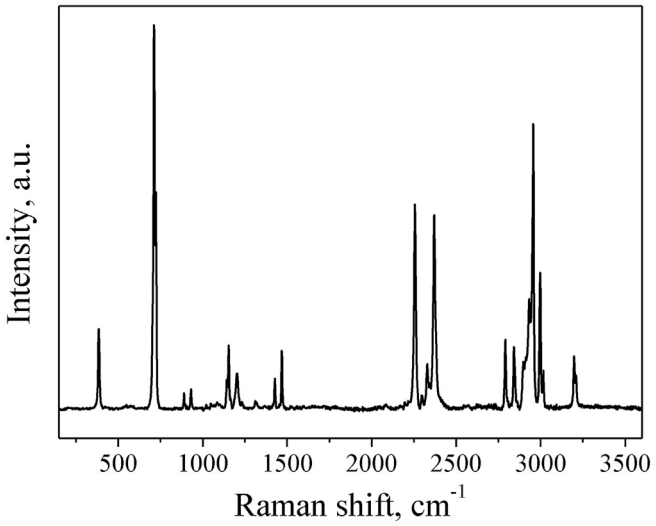

Fig. 6. Raman spectrum of $(CH_3)_2NHBH_3$ recorded under ambient conditions.

3.2. Dimethylamine borane

Raman Spectroscopy. The Raman spectrum recorded of dimethylamine borane at ambient temperature and pressure is presented in Fig. 6. First-principles calculations were again used to aid spectral interpretation, with all calculated modes found to be in agreement with experimental modes to within 5%. The characteristic Raman shifts for the B—N stretching modes (712 and 723 cm^{-1}) are somewhat lower than what was published previously [69] and they are significantly lower than those observed for methylamine borane (738 and 753 cm^{-1}, this work) and ammonia borane (784 and 800 cm^{-1} [80]) due to the different B—N bond lengths 1.596 Å [68] for the dimethylamine, 1.594 Å [51] for the methylamine and 1.58 Å for ammonia borane [83]. For mode assignments refer to Table A2 in the Supplementary Information.

Similar to the cases of ammonia borane and methylamine borane, the compression of dimethylamine borane resulted in shifts to higher wavenumber of most bands, except for the N—H stretching modes that were red-shifted upon the application of pressure (Fig. 7b), indicative of the strengthening of intermolecular

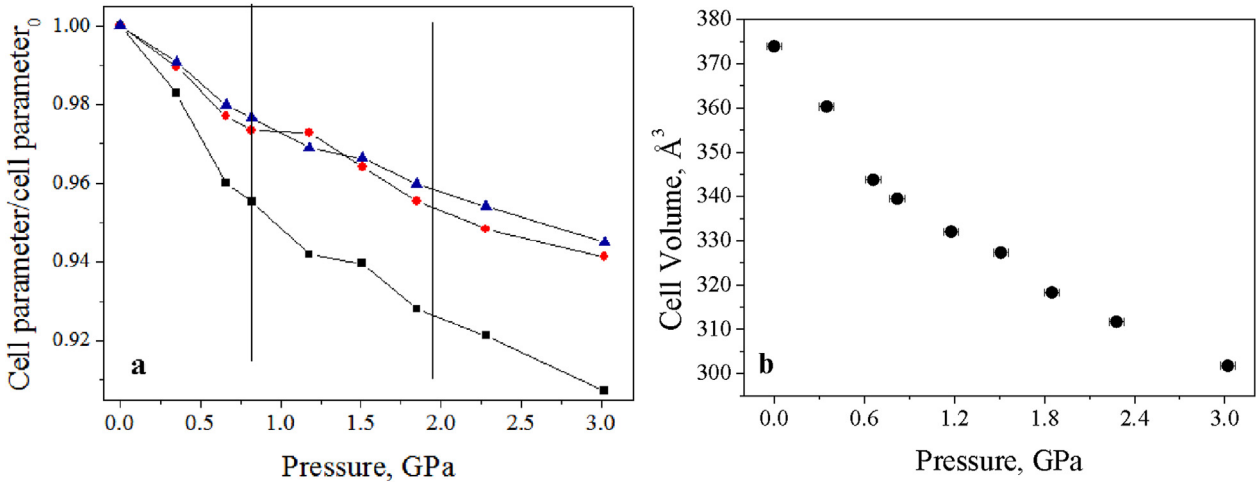

Fig. 5. **(a)** Compression plot of cell parameters for $CH_3NH_2BH_3$ as a function of pressure: black square – a/a_0, red circle: b/b_0 and blue triangle – c/c_0. Note data points are connected by straight lines as a visual guide. **(b)** Variation of the unit cell volume of $CH_3NH_2BH_3$ as a function of pressure. (For interpretation of the references to colour in this figure legend, the reader is referred to the web version of this article.)

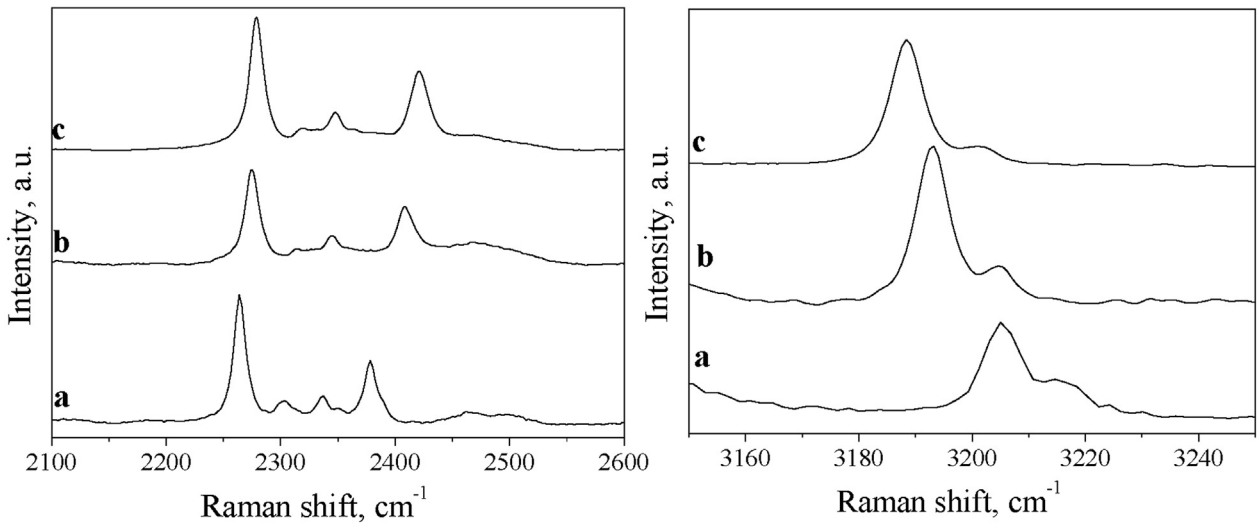

Fig. 7. From left to right: in the 2150-2600 cm^{-1} and in the 3150-3250 cm^{-1} regions at a: ambient, b: 0.7 and c: 1.0 GPa pressure.

contacts [33–36,47].

However, in contrast with the case of methylamine borane, increasing the pressure to 0.7 GPa results in apparent changes in the Raman spectrum of dimethylamine borane (see Fig. 7a). For example the peak at *ca.* 2298 cm^{-1} (a B–H stretching vibration) collapses at 0.7 GPa, together with the peak at 2345 cm^{-1}, which is assigned to a complex combination of the CH_3 deformation, NH-wagging, C–N stretching and BH_3 and CH_3 deformation modes. These differences may indicate that the material undergoes a phase transition below 0.7 GPa. However, this observation has been previously explained by different pressure dependencies of the Fermi resonance between fundamental/overtone pairs and thus has not been attributed to a phase transition [69]. In addition, the N–H and B–H vibration modes display a significant shift upon pressure increase to 0.7 GPa. It is interesting to note that in the case of ammonia borane a B–N bond shifted by 1.3% for every GPa applied [47], whereas for dimethylamine borane a staggering 2.7% shift was observed. In addition, the B–N stretching mode remained in the Raman spectrum as one doublet, displaying the ^{10}B-^{11}B isotope splitting. Given the extreme sensitivity of this band frequency to the B–N bond length [34,37,47], we can therefore safely assume that there is only one dimethylamine conformation present when the sample is compressed.

Structural Characterisation: SXPD. The structure of dimethylamine borane was first determined by S. Aldridge and co-workers at 150 K using single-crystal diffraction (Fig. 8) [68]. They found that the compound crystallises in the monoclinic $P2_1/c$ space group, which is built up from chains of the adduct molecules running

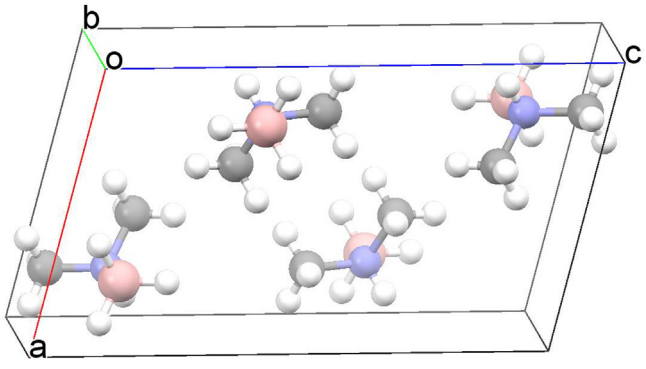

Fig. 8. Crystal packing of $(CH_3)_2NHBH_3$ at ambient pressure.

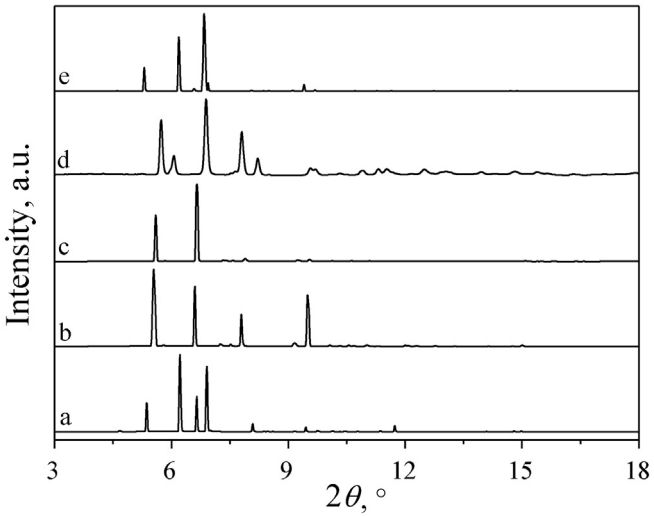

Fig. 9. Powder X-ray diffraction pattern of $(CH_3)_2NHBH_3$ at a: ambient; b: 0.8 GPa; c: 1.0 GPa; d: 3.2 GPa and at e: ambient pressure after decompression.

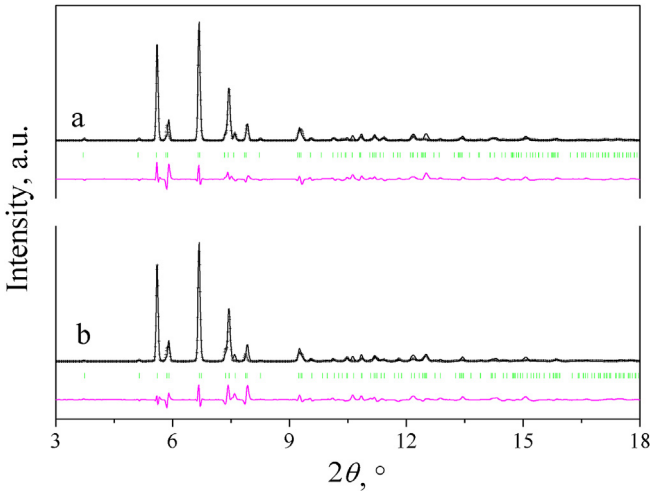

Fig. 10. X-ray powder patterns of the $(CH_3)_2NHBH_3$ under 1.0 GPa as refined in the a: *Pccn* and b: *Pbcn* space groups. Black line: observed pattern, crosses: calculated pattern, green tick marks: modelled peaks, pink line: difference of the observed and calculated patterns. (For interpretation of the references to colour in this figure legend, the reader is referred to the web version of this article.)

Table 2
Refined lattice parameters for the $(CH_3)_2NHBH_3$ at ambient pressure and 1 GPa, using the *Pccn* and *Pbcn* orthorhombic models.

	Space group	a, Å	b, Å	c, Å	β, °	V_{cell}, Å^3	Z	χ^2
150 K, ambient Single crystal [68]	$P2_1/c$	7.0452	5.8368	12.2335	104.65	486.708	4	$R = 0.042$
Room temperature, 1.0 GPa	*Pccn*	14.98 (5)	5.83 (2)	9.96 (4)	90	870	8	wR_p[a] = 0.2201
Room temperature, 1.0 GPa	*Pbcn*	14.98 (6)	5.83 (3)	9.96 (6)	90	870	8	wR_p[a] = 0.2207

[a] Background corrected.

along the *b*-axis. They demonstrated that H···H bonding links the molecules head-to-tail, shown as a bifurcated BH_2···HN interaction, with H···H distance of 2.083 and 2.202 Å [68]. The chains are relatively closely packed, with the interchain H···H linking distances being 2.562 and 2.684 Å for the shortest BH···HC and CH···HC distances, respectively [68].

In order to determine the high-pressure phase of dimethylamine borane, synchrotron powder X-ray data were collected on polycrystalline dimethylamine borane at ambient temperature, as a function of pressure up to 3.2 GPa. On raising the pressure to 0.8 GPa (see Fig. 9a and b) a dramatic change was observed in the pattern indicating the formation of a new phase. This persisted up to 3.2 GPa although with broadening of peaks, but reverted to the ambient-pressure phase on decompression. Inspection of the two-dimensional diffraction images showed that the degree of texture (preferred orientation) of the sample was substantially reduced on passing through the phase transition, indicating that a reconstructive transition had taken place. This is also reflected in the observation from Fig. 9 that the two patterns recorded at ambient pressure show some peaks with very different intensities. Dimethylamine borane is very hygroscopic and decomposes in air, thus in order to minimise this effect, the sample was only lightly ground before loading into the diamond-anvil cell. However, as a consequence of this, powder averaging for the first ambient-pressure pattern was poor. This resulted in anomalous intensities for some Bragg peaks.

It proved possible to index the pattern for the high-pressure phase recorded at 1.0 GPa to an orthorhombic crystal system with lattice parameters $a = 14.98$, $b = 5.83$, $c = 9.96$ Å. Systematic absences suggested two possible space groups: *Pccn* or *Pbcn* (Fig. 10a and b, Table 2). For the initial Rietveld refinements, atomic parameters were fixed.

From Table 2 we observe that the cell parameters, as well as the errors and *R*-factors of the two high-pressure powder refinements, are very similar.

In an attempt to resolve the identity of the space group, we pursued high-pressure single-crystal diffraction experiments, since this would provide a more accurate determination of the crystallographic systematic absences. In addition, high-quality single-crystal data may also provide some information that could contribute to the determination of hydrogen atom positions. Suitable single crystals of the dimethylamine borane were thus obtained and loaded into diamond-anvil cells using Fluorinert as the pressure-transmitting medium. The pressure was then increased to 1.2 GPa, somewhat above the transition pressure. However, it was found that the reconstructive phase transition caused the single crystals to completely disintegrate and so no useful X-ray data could be collected. Despite all our efforts, to date we have thus been unable to resolve the ambiguity between the *Pccn* and *Pbcn* space groups.

4. Conclusion

We have described the effect of pressure on the crystal structure of the potential hydrogen-storage materials methylamine borane and dimethylamine borane as studied by Raman spectroscopy and SXPD up to 3 GPa, at room temperature. The study is also supported by a DFT study, which permitted the assignment of the Raman spectra. Up to 0.6 GPa the crystal structures remain in their ambient pressure phase. Here the molecules pack so that ribbons of adducts held together *via* BH···HN bonds run along the *b*-axis of the unit cells, which are linked by weaker H···H interactions between them, directed in the *ac* planes.

Between 0.8 and 1.2 GPa, methylamine borane undergoes reversible pressure-induced structural changes, with a possibility of the existence of a second-order phase transition in the same space group. Both, our Raman and SXPD data support the strengthening of the N–H···H–B dihydrogen bonds upon compression and in the 0.8–1.2 GPa pressure range in particular.

At 0.7 GPa, dimethylamine borane undergoes a reversible, reconstructive phase transition from the monoclinic $P2_1/c$ space group. Powder X-ray diffraction allowed indexing of the resultant patterns to orthorhombic symmetry. However, despite our effort and extensive use of complimentary methods such as SXPD, single-crystal X-ray diffraction and Raman spectroscopy, we have been unable to solve the high-pressure dimehtylamine-borane structure, due to the insufficient quality SXPD data caused by preferred orientation of the material. We can thus only conclude that a reversible pressure-induced phase transition takes place as follows: monoclinic ($P2_1/c$, $a = 7.0452$, $b = 5.8368$, $c = 12.2335$, $\beta = 104.648$) → orthorhombic ($a = 14.98$, $b = 5.83$, $c = 9.96$).

Finally, we would like to emphasise the necessity of using a combination of various experimental techniques and theory to be able to identify pressure-induced phase transitions in soft materials.

Acknowledgments

P. Á. Szilágyi thanks the AXA Research Fund for funding and the Diamond Light Source for provision of synchrotron beamtime. S.H. thanks the Scottish Funding Council (SPIRIT) and QinetiQ (in support of MOD research) for contribution towards a studentship. This work made use of the facilities of HECToR, the UK's national high-performance computing service, which is provided by UoE HPCx Ltd at the University of Edinburgh, Cray Inc. and NAG Ltd, and funded by the Office of Science and Technology through EPSRC's High End Computing Programme. The authors would like to thank D. I. A. Millar for the useful discussions.

Appendix A. Supplementary data

Supplementary data related to this article can be found at http://dx.doi.org/10.1016/j.jallcom.2017.06.174.

References

[1] D.P. Broom, Hydrogen Storage Materials, the Characterisation of Their Storage Properties, Springer Verlag, 2011.
[2] P. Jena, Materials for hydrogen storage: past, present, and future, J. Phys. Chem. Lett. 2 (2011) 206–2011.
[3] L. Schlapbach, A. Züttel, Hydrogen-storage materials for mobile applications, Nature 414 (2001) 353–358.
[4] Q. Lai, M. Paskevicius, D.A. Sheppard, C.E. Buckley, A.W. Thornton, M.R. Hill,

Q. Gu, J. Mao, Z. Huang, H.K. Liu, Z. Guo, A. Banerjee, S. Chakraborty, R. Ahuja, K.-F. Aguey-Zinsou, Hydrogen storage materials for mobile and stationary applications: current state of the art, ChemSusChem 8 (2015) 2789–2825.
[5] T.K. Nielsen, F. Besenbacher, T.R. Jensen, Nanoscale 3 (2011) 2086–2098.
[6] X. Liu, H.W. Langmi, S.D. Beattie, F.F. Azenwi, G.S. McGrady, C.M. Jensen, Ti-doped $LiAlH_4$ for hydrogen storage: synthesis, catalyst loading and cycling performance, J. Am. Chem. Soc. 133 (2011) 15593–15597.
[7] M. Dornheim, N. Eigen, G. Barkhordarian, T. Klassen, R. Bormann, Tailoring hydrogen storage materials towards application, Adv. Eng. Mater. 8 (2006) 377–385.
[8] R.S. Chellappa, D. Chandra, Pressure-induced phase transformations in $LiAlH_4$, J. Phys. Chem. B 110 (2006) 11088–11097.
[9] S. Nakano, H. Fujihisa, H. Yamawaki, T. Kikegawa, Structural analysis of some high-pressure stable and metastable phases in lithium borohydride $LiBH_4$, J. Phys. Chem. C 119 (2015) 3911–3917.
[10] K. Yvon, Hydrogen in novel solid-state metal hydrides, Z. Krist. 218 (2003) 108–116.
[11] E. Rönnebro, E.H. Majzoub, Crystal structure, Raman spectroscopy, and ab initio calculations of a new bialkali alanate K_2LiAlH_6, J. Phys. Chem. B 110 (2006) 25686–25691.
[12] Y. Filinchuk, D. Chernyshov, R.J. Černý, Lightest borohydride probed by synchrotron X-ray diffraction: experiment calls for a new theoretical revision, J. Phys. Chem. C 112 (2008) 10579–10584.
[13] Y. Filinchuk, D. Chernyshov, A. Nevidomskyy, V. Dmitriev, High-pressure polymorphism as a step towards destabilization of $LiBH_4$, Angew. Chem. Int. Ed. 47 (2008) 529–532.
[14] Y. Yo, D.D. Klug, High-pressure phases of lithium borohydride $LiBH_4$: a first-principles study, Phys. Rev. B 86 (2012). #064107.
[15] R. Černý, Y. Filinchuk, H. Hagemann, K. Yvon, Magnesium borohydride: synthesis and crystal structure, Angew. Chem. Int. Ed. 46 (2007) 5765–5767.
[16] J.-H. Her, P.W. Stephens, Y. Gao, G.L. Soloveichik, J. Rijssenbeek, M. Andrus, J.-C. Zhao, Structure of unsolvated magnesium borohydride $Mg(BH_4)_2$, Acta Crystallogr. B 63 (2007) 561–568.
[17] Y. Filinchuk, R. Černý, H. Hagemann, Insight into $Mg(BH_4)_2$ with synchrotron X-ray diffraction: structure revision, crystal chemistry, and anomalous thermal expansion, Chem. Mater. 21 (2009) 925–933.
[18] O. Zavorotynska, A. El-Kharbachi, S. Deledda, B.C. Hauback, Recent progress in magnesium borohydride $Mg(BH_4)_2$: fundamentals and applications for energy storage, Int. J. Hydr. Energy 41 (2016) 14387–14403.
[19] F.H. Stephens, V. Pons, R.T. Baker, Ammonia–borane: the hydrogen source par excellence? Dalton Trans. (2007) 2613–2626.
[20] T.B. Marder, Will we soon Be fueling our automobiles with ammonia–borane? Angew. Chem. Int. Ed. 46 (2007) 8116–8118.
[21] D.J. Heldebrant, A. Karkamkar, J.C. Linehan, T. Autrey, Synthesis of ammonia borane for hydrogen storage applications, Energy Environ. Sci. 1 (2008) 156–160.
[22] B. Peng, J. Chen, Ammonia borane as an efficient and lightweight hydrogen storage medium, Energy Environ. Sci. 1 (2008) 479–483.
[23] J.-F. Petit, P. Miele, U.B. Demirci, Ammonia borane H_3N-BH_3 for solid-state chemical hydrogen storage: different samples with different thermal behaviors, Int. J. Hydr. Energy 41 (2016) 15462–15470.
[24] F. Baitalow, J. Baumann, G. Wolf, K. Jaenicke-Rößler, G. Leitner, Thermal decomposition of B–N–H compounds investigated by using combined thermoanalytical methods, Thermochim. Acta 391 (2002) 159–168.
[25] A. Gutowska, L. Li, Y. Shin, C.M. Wang, X.S. Li, J.C. Linehan, R.S. Smith, B.D. Kay, B. Schmid, W. Shaw, M. Gutowski, T. Autrey, Nanoscaffold mediates hydrogen release and the reactivity of ammonia borane, Angew. Chem. Int. Ed. 44 (2005) 3578–3582.
[26] S. Sepehri, A. Feaver, W.J. Shaw, C.J. Howard, T. Autrey, Spectroscopic studies of dehydrogenation of ammonia borane in carbon cryogel, J. Phys. Chem. B 111 (2007) 14285–14289.
[27] Z. Li, G. Zhu, G. Lu, S. Qiu, X. Yao, Ammonia borane confined by a Metal–Organic framework for chemical hydrogen storage: enhancing kinetics and eliminating ammonia, J. Am. Chem. Soc. 132 (2010) 1490–1491.
[28] J. Richard, S. León Cid, J. Rouquette, A. van der Lee, S. Bernard, J. Haines, Pressure-induced insertion of ammonia borane in the siliceous zeolite, Silicalite-1F, J. Phys. Chem. C 120 (2016) 9334–9340.
[29] S.-W. Lai, H.-L. Lin, T.L. Yu, L.-P. Lee, B.-J. Weng, Hydrogen release from ammonia borane embedded in mesoporous silica scaffolds: SBA-15 and MCM-41, Int. J. Hydr. Energy 37 (2012) 14393–14404.
[30] M. Chandra, Q. Xu, Dissociation and hydrolysis of ammonia-borane with solid acids and carbon dioxide: an efficient hydrogen generation system, J. Power Sources 159 (2006) 855–860.
[31] M.E. Bluhm, M.G. Bradley, R. Butterick III, U. Kusari, L.G. Sneddon, Amine-borane-based chemical hydrogen Storage: enhanced ammonia borane dehydrogenation in ionic liquids, J. Am. Chem. Soc. 128 (2006) 7748–7749.
[32] C. Sun, A. Du, X. Yao, S.C. Smith, Adsorption and dissociation of ammonia borane outside and inside single-walled carbon nanotubes: a density functional theory study, J. Phys. Chem. C 115 (2011) 12580–12585.
[33] S. Trudel, D.F.R. Gilson, High-pressure Raman spectroscopic study of the Ammonia–Borane complex. Evidence for the dihydrogen bond, Inorg. Chem. 42 (2003) 2814–2816.
[34] Y. Lin, W.L. Mao, V. Drozd, J. Chen, L.L. Daemen, Raman spectroscopy study of ammonia borane at high pressure, J. Chem. Phys. 129 (2008) 234509.
[35] J. Nylén, T. Sato, E. Soignard, J.L. Yarger, E. Stoyanov, U. Häussermann, Thermal decomposition of ammonia borane at high pressures, J. Chem. Phys. 131 (2010) 104506.
[36] S. Xie, Y. Song, Z. Liu, In situ high-pressure study of ammonia borane by Raman and IR spectroscopy, Can. J. Chem. 87 (2009) 1235–1247.
[37] Y. Filinchuk, A.H. Nevidomskyy, D. Chernyshov, V. Dmitriev, High-pressure phase and transition phenomena in ammonia borane NH_3BH_3 from x-ray diffraction, Landau theory, and ab initio calculations, Phys. Rev. B 79 (2009) 214111–214122.
[38] P. Vajeeston, P. Ravindran, A. Kjehus, H. Fjellvåg, Structural stability of alkali boron tetrahydrides ABH_4 (A = Li, Na, K, Rb, Cs) from first principle calculation, J. Alloy. Compd. 387 (2005) 97–104.
[39] Y. Zhao, D. He, J. Qian, C. Pantea, K.A. Lokshin, J. Zhang, L.L. Daemen, Advances in High-pressure Technology for Geophysical Applications, Elsevier B.V., 2005, pp. 461–474.
[40] R.S. Kumar, X. Ke, J. Zhang, Z. Lin, S.C. Vogel, M. Hartl, S. Sinogelkin, L. Daemen, A.L. Corneliu, C. Chen, Y. Zhao, Pressure induced structural changes in the potential hydrogen storage compound ammonia borane: a combined X-ray, neutron and theoretical investigation, Chem. Phys. Lett. 495 (2010) 203–207.
[41] L. Wang, K. Bao, X. Meng, X. Wang, T. Jiang, T. Cuia, B. Liu, G. Zou, Structural and dynamical properties of solid ammonia borane under high pressure, J. Chem. Phys. 134 (2011) 024517.
[42] C.A. Morrison, M.M. Siddick, Dihydrogen bonds in solid BH_3NH_3, Angew. Chem. Int. Ed. 43 (2004) 4780–4782.
[43] Ch. B. Lingam, K.R. Babu, S.P. Tewari, G. Vaitheeswaran, Structural, electronic, bonding, and elastic properties of NH_3BH_3: a density functional study, J. Comp. Chem. 32 (2011) 1734–1742.
[44] L. Wang, K. Bao, X. Meng, X. Wang, T. Jiang, T. Cui, B. Liu, G. Zou, Structural and dynamical properties of solid ammonia borane under high pressure, J. Chem. Phys. 134 (2011) 024517.
[45] M. Ramzan, R. Ahuja, High pressure and temperature study of hydrogen storage material BH_3NH_3 from ab initio calculations, J. Phys. Chem. Sol. 71 (2010) 1137–1139.
[46] Y. Yao, X. Yong, J.S. Tse, M.J. Greschner, Dihydrogen bonding in compressed ammonia borane and its roles in structural stability, J. Phys. Chem. C 118 (2014) 29591–29598.
[47] R. Custalcean, Z.A. Dreger, Dihydrogen bonding under high Pressure: a Raman study of BH_3NH_3 molecular crystal, J. Phys. Chem. B 107 (2003) 9231–9235.
[48] J. Chen, H. Couvya, H. Liub, V. Drozda, L.L. Daemenc, Y. Zhaoc, C.-C. Kaod, In situ X-ray study of ammonia borane at high pressures, Int. J. Hydr. Energy 35 (2010) 11064–11070.
[49] Y. Lin, H. Ma, C. Wesley Matthews, B. Kolb, S. Sinogeikin, T. Thonhauser, W.L. Mao, Experimental and theoretical studies on a high pressure monoclinic phase of ammonia borane, J. Phys. Chem. C 116 (2012) 2172–2178.
[50] S. Najiba, J. Chen, V. Drozd, A. Durygin, Y. Sun, Tetragonal to orthorhombic phase transition of ammonia borane at low temperature and high pressure, J. Appl. Phys. 111 (2011) 112618.
[51] M.E. Bowden, I.W.M. Brown, G.J. Gainsford, H. Wong, Structure and thermal decomposition of methylamine borane, Inorg. Chim. Acta 361 (2008) 2147–2153.
[52] D.J. Grant, M.H. Matis, K.D. Anderson, D.M. Camaioni, S.R. Neufeldt, C.F. Lane, D.A. Dixon, Thermochemistry for the dehydrogenation of methyl-substituted ammonia borane compounds, J. Phys. Chem. A 113 (2009) 6121–6132.
[53] Y. Chen, J.L. Fulton, J.C. Linehan, T. Autrey, In situ XAFS and NMR study of rhodium-catalyzed dehydrogenation of dimethylamine borane, J. Am. Chem. Soc. 127 (2005) 3254–3255.
[54] C.-H. Sun, X.-D. Yao, A.-J. Du, L. Li, S. Smith, G.-Q. Lu, Computational study of methyl derivatives of ammonia borane for hydrogen storage, Phys. Chem. Chem. Phys. 10 (2008) 6104–6106.
[55] T. Miyazaki, Y. Tanabe, M. Yuki, Y. Miyake, Y. Nishibayashi, Synthesis of group IV (Zr, Hf)–Group VIII (Fe, Ru) heterobimetallic complexes bearing metallocenyl diphosphine moieties and their application to catalytic dehydrogenation of Amine–Boranes, Organometallics 30 (2011) 2394–2404.
[56] M.S. Hill, G. Kociok-Köhn, T.P. Robinson, Group 3-centred dehydrocoupling of $Me_2NH{\cdot}BH_3$, Chem. Comm. 46 (2010) 7587–7589.
[57] M.E. Sloan, A. Staubitz, T.J. Clark, C.A. Russel, G.C. Lloyd-Jones, I. Manners, Homogeneous catalytic dehydrocoupling/dehydrogenation of Amine–Borane adducts by early transition metal, group 4 metallocene complexes, J. Am. Chem. Soc. 132 (2010) 3831–3841.
[58] Y. Kawano, M. Uruichi, M. Shimoi, S. Taki, T. Kawaguchi, T. Kakizawa, H. Ogino, Dehydrocoupling reactions of Borane–Secondary and –Primary amine adducts catalyzed by Group-6 carbonyl complexes: formation of aminoboranes and borazines, J. Am. Chem. Soc. 131 (2009) 14946–14957.
[59] Y. Jiang, O. Blacque, T. Fox, C.M. Frech, H. Berke, Development of rhenium catalysts for amine borane dehydrocoupling and transfer hydrogenation of olefins, Organometallics 28 (2009) 5493–5504.
[60] M. Käß, A. Friedrich, M. Drees, S. Schneider, Ruthenium complexes with cooperative PNP ligands: bifunctional catalysts for the dehydrogenation of ammonia–borane, Angew. Chem. Int. Ed. 48 (2009) 905–907.
[61] B.L. Conley, T. Williams, J., Dehydrogenation of ammonia-borane by Shvo's catalyst, Chem. Comm. 46 (2010) 4815–4817.
[62] A. Staubitz, M.E. Sloan, A.P.M. Robertson, A. Friedrich, A. Schneider, P.J. Gates, J. Schmedt auf der Günne, I. Manners, Catalytic Dehydrocoupling/Dehydrogenation of N-Methylamine-Borane and Ammonia-Borane: synthesis and Characterization of High Molecular Weight Polyaminoboranes, J. Am. Chem. Soc. 132 (2010) 13332–13345.

[63] S.-K. Kim, W.-S. Han, T.-J. Kim, T.-Y. Kim, S.W. Nam, M. Mitoraj, L. Pieko, A. Michalak, A.-J. Hwang, S.O. Kang, Palladium catalysts for dehydrogenation of ammonia borane with preferential B–H activation, J. Am. Chem. Soc. 132 (2010) 9954–9955.
[64] S.S. Mal, F.H. Stephens, R.T. Baker, Transition metal catalysed dehydrogenation of amine-borane fuel blends, Chem. Comm. 47 (2011) 2922–2924.
[65] G. Alcaraz, S. Sabo-Etienne, Coordination and dehydrogenation of amine-boranes at metal centers, Angew. Chem. Int. Ed. 49 (2010) 7170–7179.
[66] Z. Mehmet, M. Tristany, K. Philippot, K. Fajerweg, S. Özkar, B. Chaudret, Aminopropyltriethoxysilane stabilized ruthenium(0) nanoclusters as an isolable and reusable heterogeneous catalyst for the dehydrogenation of dimethylamine–borane, Chem. Comm. 46 (2010) 2938–2940.
[67] E.Ü. Barın, M. Masjedi, S. Özkar, A new homogeneous catalyst for the dehydrogenation of dimethylamine borane starting with ruthenium(III) acetylacetonate, Materials 8 (2015) 3155–3167.
[68] A. Aldridge, A.J. Downs, C.Y. Tang, S. Parsons, M.C. Clarke, R.D.L. Johnstone, H.E. Robertson, D.W.H. Rankin, D.A. Wann, Structures and aggregation of the Methylamine–Borane molecules, $Me_nH_3{-}nN{\cdot}BH_3$ (n = 1–3), studied by X-ray diffraction, gas-phase electron diffraction, and quantum chemical calculations, J. Am. Chem. Soc. 131 (2009) 2231–2243.
[69] R.G. Potter, M. Somayazulu, G. Cody, R.J. Hemley, High pressure equilibria of dimethylamine borane, dihydridobis(dimethylamine)boron(III) tetrahydridoborate(III), and hydrogen, J. Phys. Chem. C 118 (2014) 7280–7287.
[70] L. Merrill, W.A. Bassett, Miniature diamond anvil pressure cell for single crystal x-ray diffraction studies, Rev. Sci. Instrum. 45 (1974) 290–295.
[71] G.J. Piermarini, S. Block, J.D. Barnett, R.A. Forman, Calibration of the pressure dependence of the R1 ruby fluorescence line to 195 kbar, J. Appl. Phys. 46 (1975) 2774–2781.
[72] S.P. Thompson, J.E. Parker, J. Potter, T.P. Hill, A. Birt, T.M. Cobb, F. Yuan, C.C. Tang, Beamline I11 at Diamond: a new instrument for high resolution powder diffraction, Rev. Sci. Instrum. 80 (2009) 075107.
[73] A.P. Hammersley, S.O. Svensson, M. Hanfland, A.N. Fitch, D. Hausermann, Two-dimensional detector software: from real detector to idealised image or two-theta scan, High. Press. Res. 14 (1996) 235–248.
[74] R. Shirley, The Crysfire 2002 System for Automatic Powder Indexing: User's Manual, The Lattice Press, 41 Guildford Park Avenue, Guildford, Surrey GU2 7NL, England, 2002.
[75] A.C. Larson, R.B. von Dreele, General Structure Analysis System (GSAS), Los Alamos National Laboratory, Los Alamos, NM, 1994.
[76] V. Favre-Nicolin, R. Cerny, FOX, 'free objects for crystallography': a modular approach to ab initio structure determination from powder diffraction, J. Appl. Cryst. 35 (2002) 734–743.
[77] P.W. Betteridge, J.R. Carruthers, R.I. Cooper, K. Prout, D.J. Watkin, CRYSTALS version 12: software for guided crystal structure analysis, J. Appl. Cryst. 36 (2003) 1487.
[78] M.D. Segall, P.J.D. Lindan, M.J. Probert, C.J. Pickard, P.J. Hasnip, S.J. Clark, M.C. Payne, First-principles simulation: ideas, illustrations and the CASTEP code, J. Phys. Condens. Matter 14 (2002) 2717–2744.
[79] Jmol: an open-source Java viewer for chemical structures in 3D. http://www.jmol.org/.
[80] N.J. Hess, M.E. Bowden, V.M. Parvanov, C. Mundy, S.M. Kathmann, G.K. Schenter, T. Autrey, Spectroscopic studies of the phase transition in ammonia borane: Raman spectroscopy of single crystal NH_3BH_3 as a function of temperature from 88 to 330 K, J. Chem. Phys. 128 (2008) 034508.
[81] C.F. Macrae, L.J. Bruno, J.A. Chisholm, P.R. Edgington, P. McCabe, E. Pidcock, L. Rodriguez-Monge, R. Taylor, J. van de Streek, P.A. Wood, Mercury CSD 2.0-new features for the visualization and investigation of crystal structures, J. Appl. Crystallogr. 41 (2008) 466–470.
[82] T. Varga, A.P. Wilkinson, R.J. Angel, Fluorinert as a pressure-transmitting medium for high-pressure diffraction studies, J. Rev. Sci. Instrum. 74 (2003) 4564–4566.
[83] W.T. Klooster, T.F. Koetzle, P.E.M. Siegbahn, T.B. Richardson, R.H. Crabtree, Study of the N–H···H–B dihydrogen bond including the crystal structure of BH_3NH_3 by neutron diffraction, J. Am. Chem. Soc. 121 (1999) 6337–6343.